# 2-D inverse scattering analysis using pure SH wave for delamination in carbon fiber reinforced plastic


**†Takahiro Saitoh[1], Takashi Onodera[1], Akira Furukawa[2] and *Sohichi Hirose[2]**

[1]Department of Civil and Environmental Engineering, Gunma University, Japan
[2]Department of Civil and Environmental Engineering, Tokyo Institute of Technology, Japan

*Presenting author: hirose.s.aa@m.titech.ac.jp
†Corresponding author: t-saitoh@gunma-u.ac.jp



## Abstract

In this paper, a linearized inverse scattering technique with the aid of the convolution quadrature time-domain boundary element method (CQBEM) has been developed for the reconstruction of a delamination in carbon fiber reinforced plastic (CFRP) with anisotropic property. The CQBEM is utilized to obtain scattered wave data from a delamination in CFRP. The wave forms obtained by the CQBEM are adequately treated to implement the shape reconstruction of a delamination in CFRP. The Kirchhoff approximation is applied to the unknown delamination opening displacement. A far-field approximation of the 2-D fundamental solution in frequency-domain for general anisotropic elastodynamics is used for the proposed inverse scattering formulation. Numerical examples for a delamination in various types of CFRPs are shown to verify the proposed method.



Keywords: **Time-domain BEM, inverse scattering analysis, anisotropic elastodynamics, carbon FRP**


## Introduction

Some anisotropic materials have attracted lots of interest in the fields of the mechanical and civil engineering in recent years. The carbon fiber reinforced plastic (CFRP) is known as one of the typical anisotropic materials, and is generally used as a material of construction for bridges and aircrafts, because the FRP has the characteristics of high tension strength, corrosive resistance and light weight. The ultrasonic non-destructive testing is most widely used in order to provide evidence of safety for structural materials. The exact identification of position, size, and shape of a defect in materials is an important factor for structural monitoring and health diagnostics. Defect shape reconstruction methods for materials have been developed by several researchers since several years ago [1][2]. The inverse scattering is an effective defect shape reconstruction method, and has been applied to many engineering problems [3][4][5]. However, no numerical example using the inverse scattering method can be seen for the reconstruction of a defect in CFRP with the anisotropic property. The acoustic anisotropic property makes it difficult for the nondestructive engineers to evaluate a defect. Therefore, in this study, an inverse scattering technique is developed for a defect shape reconstruction for CFRP with anisotropic property. The pure SH wave mode is only considered in this study for simplicity. The convolution quadrature time-domain boundary element method (CQBEM) [6][7][8][9] is utilized to obtain the scattered wave data from a delamination in a CFRP, which is required for the implementation of the inverse scattering formulation. The proposed inverse scattering formulation is achieved in the frequency-domain. Therefore, the scattered wave data in frequency-domain are calculated by using the Fourier transform of those in time-domain

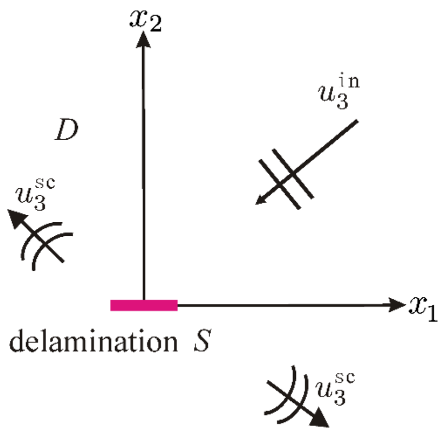


**Figure 1 Analysis model.**

obtained by CQBEM. In the following sections, the problem statement and proposed inverse scattering formulation are discussed. Some numerical results for the shape reconstruction of a delamination in various types of CFRPs are presented. Finally, some comments and our future research plans are remarked.

## Problem statement

The proposed 2-D inverse scattering formulation using pure SH wave is based on the Kirchhoff approximation [10]. Some important equations for the study on this inverse scattering for a delamination in CFRP are shown in this section, because of the page limitation. In this research, we assume that the pure SH wave is generated by the interaction between the incident wave $u_3^{\mathrm{in}}(\boldsymbol{x}, t)$ and a delamination $S$ in CFRP, as shown in Fig.1, namely, the elastic waves generated in CFRP can be decomposed into the pure SH wave and in-plane wave modes. The equation of motion and constitutive equation at the position $\boldsymbol{x}$ and time $t$ for the anisotropic elastodynamics are defined as follows:

$$\rho \ddot{u}_i(\boldsymbol{x}, t) = \sigma_{ij,j}(\boldsymbol{x}, t) \tag{1}$$

$$\sigma_{ij}(\boldsymbol{x}, t) = C_{ijkl} u_{k,l}(\boldsymbol{x}, t) \tag{2}$$

where $\sigma_{ij}$ is the stress, $\rho$ is the density of CFRP, $u_i(\boldsymbol{x}, t)$ is the displacement, $(\ )_{,i}$ is the partial derivative with respect to $\partial/\partial x_i$, and $(\dot{\ })$ is the time derivative. In addition, $C_{ijkl}$ is the elastic constant. The fourth order elastic constant $C_{ijkl}$ is related to the Voigt notation elastic constant $C_{IJ}(i, j = 1, \ldots, 6)$ [10] expressed by

$$I = \begin{cases} i & : i = j \\ 9 - (i + j) & : i \neq j \end{cases}, \quad J = \begin{cases} k & : k = l \\ 9 - (k + l) & : k \neq l \end{cases}. \tag{3}$$

## 2-D inverse scattering formulation using pure SH wave

The delamination must be carefully taken into consideration during CFRPs in-service period. In the frequency domain, the boundary integral equation for the scattered wave $u_3^{sc}(\boldsymbol{x}, \omega)$ with the time-harmonic frequency $\omega$ in infinite domain $D$, as shown in Fig.1, can be written as follows:

$$u_3^{sc}(\boldsymbol{x},\omega) = -\int_S C_{3\alpha 3\beta} e_\alpha(\boldsymbol{y}) \frac{\partial U_{33}(\boldsymbol{x},\boldsymbol{y},\omega)}{\partial y_\beta}[u_3(\boldsymbol{y},\omega)]dS_y \tag{4}$$

where $[u]_3$ and $e_\alpha$ show the delamination opening displacement for anti-plane direction and the unit normal vector with respect to the outer normal direction on $\boldsymbol{y}$, respectively. In addition, $U_{33}(\boldsymbol{x},\boldsymbol{y},\omega)$ denotes the traction fundamental solution for 2-D anti-plane anisotropic elastodynamics in frequency-domain. The fundamental solution $U_{33}(\boldsymbol{x},\boldsymbol{y},\omega)$, derived by Wang and Achenbach [12], is given as follows:

$$U_{33}(\boldsymbol{x},\boldsymbol{y},\omega) = \frac{1}{8\pi^2}\int_{|\boldsymbol{n}|=1} \frac{1}{\rho c^2(\boldsymbol{n})} \phi(k(\boldsymbol{n})|\boldsymbol{n}\cdot(\boldsymbol{x}-\boldsymbol{y})|)d\boldsymbol{n} \tag{5}$$

where $c(\boldsymbol{n})$ is the phase velocity with respect to the direction $\boldsymbol{n}$ over the unit sphere and $k$ is the wave number defined by $k(\boldsymbol{n}) = \omega/c(\boldsymbol{n})$. The fundamental solution $U_{33}(\boldsymbol{x},\boldsymbol{y},\omega)$ involves the numerical integration over the unit circle with respect to $|\boldsymbol{n}| = 1$. The function $\phi(\xi)$ is defined by

$$\phi(\xi) = i\pi e^{i\xi} - 2\{\cos(\xi)\,\mathrm{ci}(\xi) + \sin(\xi)\,\mathrm{si}(\xi)\}. \tag{6}$$

In eq. (6), the functions si(ξ) and ci(ξ) are Sine and Cosine integrals, respectively, which are defined as follows:

$$\mathrm{si}(\xi) = -\int_\xi^\infty \frac{\sin(s)}{s}ds\,, \qquad \mathrm{ci}(\xi) = -\int_\xi^\infty \frac{\cos(s)}{s}ds. \tag{7}$$

The numerical evaluation of the integration over the unit sphere in eq. (5) is very time-consuming. Therefore, a far-field approximation is introduced to decrease the required computational time. In addition, the use of a far-field approximation allows us to achieve the inverse scattering formulation. If the observation point $\boldsymbol{x}$ is far enough from the source point $\boldsymbol{y}$, the fundamental solution $U_{33}(\boldsymbol{x},\boldsymbol{y},\omega)$ can be approximated by using the stationary phase method as follows:

$$\begin{aligned} U_{33}(\boldsymbol{x},\boldsymbol{y},\omega) = &\frac{i}{C_{44}}\sqrt{\frac{1}{8\pi k_0|\boldsymbol{x}||f''(\varphi^s)|}}S^2(\varphi^s) \\ &\cdot \exp[ik_0(|\boldsymbol{x}| - \hat{\boldsymbol{x}}\cdot\boldsymbol{y})f(\varphi^s) + i\frac{\pi}{4}\mathrm{sgn}\{f''(\varphi^s)\}] \end{aligned} \tag{8}$$

where $\hat{\boldsymbol{x}}$ is the unit vector of $\boldsymbol{x}$ and $k_0$ is given by $k_0 = \omega/c_0$. $c_0$ is given by $c_0 = \sqrt{C_{44}/\rho}$. $\varphi^s$ and $\psi$ satisfy $f'(\varphi^s) = 0$ and $(\cos\psi, \sin\psi) = (\boldsymbol{x}-\boldsymbol{y})/|\boldsymbol{x}-\boldsymbol{y}|$, respectively. In addition, $S(\varphi) = c_0/c(\varphi)$ and, $f(\varphi) = S(\varphi)\cos(\varphi - \psi)$. The symbol "sgn" shows the sign function. Equation (8) is the far-field approximation of the fundamental solution $U_{33}(\boldsymbol{x},\boldsymbol{y},\omega)$. Substituting eq. (8) into eq. (4), we can obtain

$$
\begin{aligned}
u_3^{sc}(\boldsymbol{x},\omega) = &-\frac{f(\varphi^s)}{C_{44}}\sqrt{\frac{k_0}{8\pi|\boldsymbol{x}||f''(\varphi^s)|}}S^2(\varphi^s) \\
&\cdot \exp\left[ik_0|\boldsymbol{x}|f(\varphi^s) + i\frac{\pi}{4}\mathrm{sgn}\{f''(\varphi^s)\}\right] \\
&\cdot \int_S e_\alpha(\boldsymbol{y})\exp\{-ik_0 f(\varphi^s)\hat{\boldsymbol{x}}\cdot\boldsymbol{y}\}\,[u_3(\boldsymbol{y},\omega)]dS_y.
\end{aligned} \tag{9}
$$

In eq. (9), the delamination opening displacement $[u_3(\boldsymbol{y},\omega)]$ is unknown. Therefore, $[u_3(\boldsymbol{y},\omega)]$ can be approximated by using the Kirchhoff approximation, which approximates the unknown delamination opening displacement as the sum of the incident wave $u_3^{in}(\boldsymbol{x},\omega)$ and the reflected wave from the delamination. In addition, the singular function $\gamma(\boldsymbol{y})$, which has the characteristic of

$$
\int_D \gamma(\boldsymbol{y})dV_y = \int_S dS_y, \tag{10}
$$

is considered. Applying the Kirchhoff approximation to eq. (9), and using both Gauss's divergence theorem and the singular function $\gamma(\boldsymbol{y})$ defined in eq. (10) yield the following equation:

$$
\begin{aligned}
u_3^{sc}(\boldsymbol{x},\omega) = &\frac{if(\varphi^s)F(\omega)}{C_{44}}\sqrt{\frac{k_0}{2\pi|\boldsymbol{x}||f''(\varphi^s)|}}C_{3\alpha3\beta}\hat{x}_\beta S^2(\varphi^s)(k_0 f(\varphi^s)\hat{x}_\alpha - k\hat{d}_\alpha^{in}) \\
&\cdot \exp\left[ik_0|\boldsymbol{x}|f(\varphi^s) + i\frac{\pi}{4}\mathrm{sgn}\{f''(\varphi^s)\}\right] \\
&\cdot \int_D \gamma(\boldsymbol{y})\exp[-i\{k_0 f(\varphi^s)\hat{\boldsymbol{x}} - k\hat{\boldsymbol{d}}^{in}\}\cdot\boldsymbol{y}]dV_y
\end{aligned} \tag{11}
$$

where $\hat{\boldsymbol{d}}^{\mathrm{in}}$ denotes the propagation vector of the incident wave. In eq. (11), the Ricker wavelet [13] is considered as the incident wave $u_3^{in}(\boldsymbol{x},\omega)$. The Ricker wave in frequency-domain, $F(\omega)$, is defined by

$$
F(\omega) = -\frac{\sqrt{2\pi}\omega^2\exp(i\omega t_s)}{2\exp(\omega^2/\omega_p^2)\omega_p^3} \tag{12}
$$

where $\omega_p$ and $t_s$ show the peak frequency and peak location of the Ricker wavelet, respectively. In eq. (11), the singular function $\gamma(\boldsymbol{y})$ is the Fourier transform with respect to $K = k_0 f(\varphi^s)\hat{\boldsymbol{x}} - k\hat{\boldsymbol{d}}^{\mathrm{in}}$. Therefore, the singular function $\gamma(\boldsymbol{y})$, which shows the delamination surface, can be obtained by the inverse Fourier transform as follows:

$$
\begin{aligned}
\gamma(\boldsymbol{y}) = -iC_{44}\int_0^{2\pi}\int_0^{\infty}&\left[\frac{f(\varphi^s)}{c_0} - \frac{1}{c}\cos(\psi - \psi^{in})\right] \\
&\cdot\frac{u_3^{sc}(\boldsymbol{x},\omega)}{F(\omega)C_{3\alpha3\beta}\hat{x}_\beta S^2(\varphi^s)\left(k_0 f(\varphi^s)\hat{x}_\alpha - k\hat{d}_\alpha^{in}\right)}
\end{aligned} \tag{13}
$$

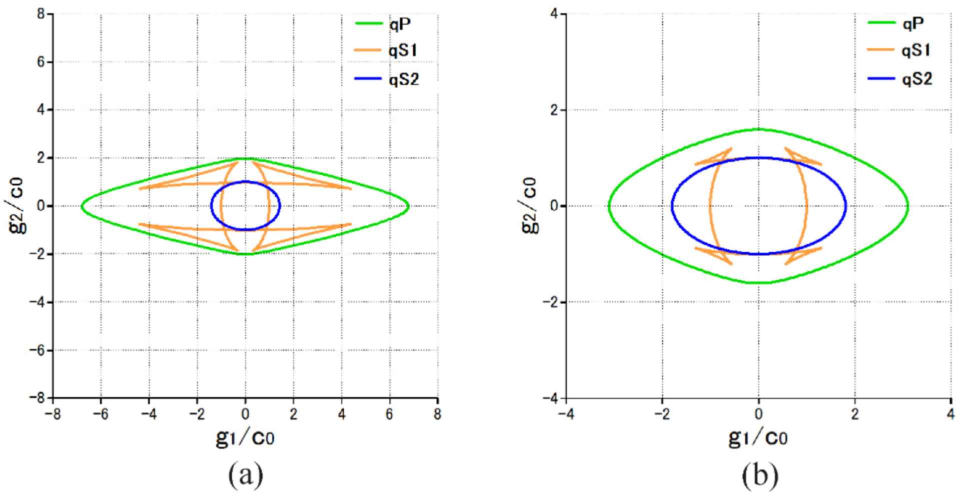


**Figure 2 Group velocity curves for (a) unidirectional CFRP (b) quasi-isotropic CFRP.**

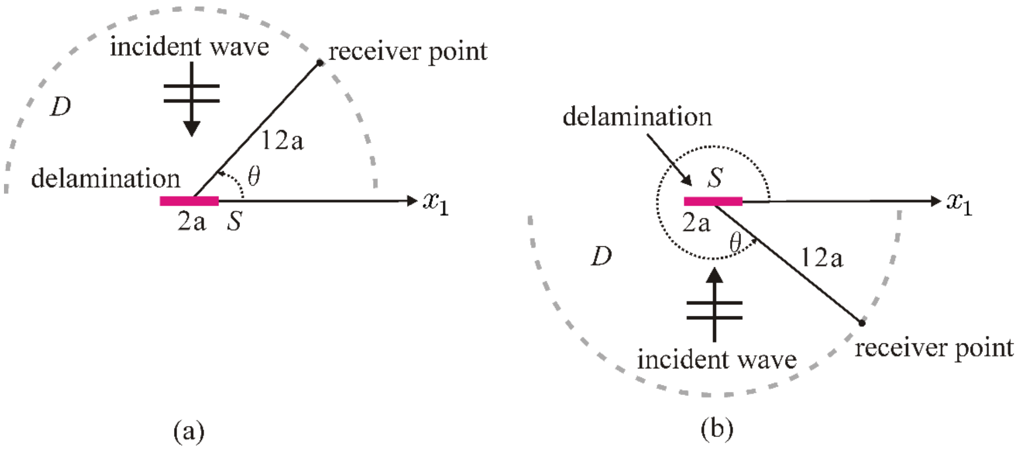


**Figure 3 Forward and inverse scattering analysis models (a) downward and (b) upward incidences.**

$$\cdot \sqrt{\frac{k_0|\boldsymbol{x}||f''(\varphi^s)|}{8\pi^3}} \exp\left[-ik_0|\boldsymbol{x}|f(\varphi^s) - i\frac{\pi}{4}\mathrm{sgn}\{f''(\varphi^s)\}\right]$$
$$\cdot \exp[i\{k_0 f(\varphi^s)\hat{\boldsymbol{x}} \cdot \boldsymbol{y} - k\widehat{\boldsymbol{d}}^{\mathrm{in}} \cdot \boldsymbol{y}\}] d\omega d\psi$$

where $\psi^{in}$ is the incident wave angle. The shape reconstruction of the delamination is implemented by the calculation of the right-hand side of eq. (13).

## Numerical results

In this section, some numerical results for the shape reconstruction of a delamination in two types of CFRPs are demonstrated by using the proposed method. The two types of CFRPs are unidirectional and quasi-isotropic CFRPs. The elastic constants of them are given in the normalized form by $C_{44}$ as follows:

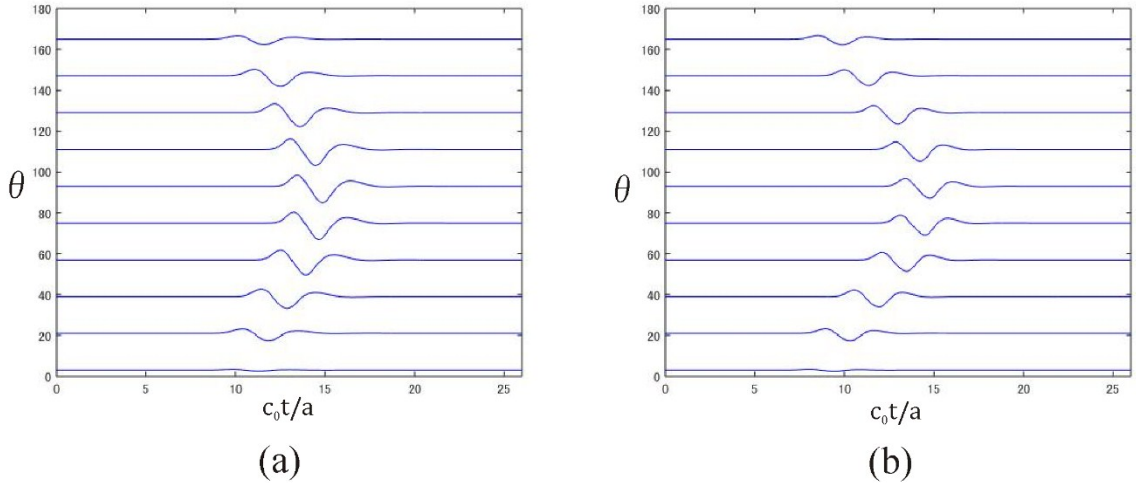


**Figure 4 Scattered wave forms $u_3^{sc}(\boldsymbol{x},\boldsymbol{t})$ obtained by CQBEM for the case of (a) unidirectional CFRP (b) quasi-isotropic CFRP.**

$$\frac{C_{\alpha\beta}}{C_{44}} = \begin{pmatrix} 45.914 & 1.829 & 41.874 & 0 & 0 & 0 \\ & 3.977 & 1.829 & 0 & 0 & 0 \\ & & 45.914 & 0 & 0 & 0 \\ & & & 1.0 & 0 & 0 \\ & \text{sym.} & & & 2.02 & 0 \\ & & & & & 1.0 \end{pmatrix} \text{(unidirectional CFRP)} \tag{14}$$

$$\frac{\boldsymbol{C_{\alpha\beta}}}{\boldsymbol{C_{44}}} = \begin{pmatrix} 9.63 & 0.77 & 4.0 & 0 & 0 & 0 \\ & 2.54 & 0.77 & 0 & 0 & 0 \\ & & 9.63 & 0 & 0 & 0 \\ & & & 1.0 & 0 & 0 \\ & \text{sym.} & & & 3.24 & 0 \\ & & & & & 1.0 \end{pmatrix} \text{(quasi-isotropic CFRP)} \tag{15}$$

Figure 2(a) and (b) show the group velocity curves for unidirectional CFRP and quasi-isotropic CFRP, respectively. As shown in Fig.2, three distinct waves, the qP wave (longitudinal wave), and qS1 and qS2 waves (shear waves), exist in each CFRP. In addition, the qP wave, which is faster than qS1 and qS2 waves, are observed. The velocity of the qP wave for the horizontal direction is faster than that for the vertical direction, due to the anisotropic property. In this analysis, the qS2 wave, which is called pure SH wave, is used to reconstruct a delamination in CFRPs. The scattered wave data $u_3^{sc}(\boldsymbol{x},\omega)$ of eq. (13) can be calculated by using the Fourier transform of $u_3^{sc}(\boldsymbol{x},t)$ obtained by the CQBEM.

*Forward analysis results obtained by CQBEM*

The results for 2-D elastic wave scattering by a delamination with the length $2a$ in CFRPs are demonstrated in this section. Figure 3 shows the forward analysis model and the scattered waves $u_3^{sc}(\boldsymbol{x},\omega)$ at several receiver points, which are away from the center of the delamination by $12a$, are calculated with the aid of the CQBEM. In this analysis, two cases which are downward and upward incidences for the delamination, as shown in Fig.3(a) and (b), respectively, are considered. The delamination is discretized by the piecewise constant boundary elements and the number of boundary elements $M$ is given by $M = 20$. The time increment $c_0t/a$, the number of total time steps $N$, and the central frequency of the Ricker wavelet $\omega_p$ are given by

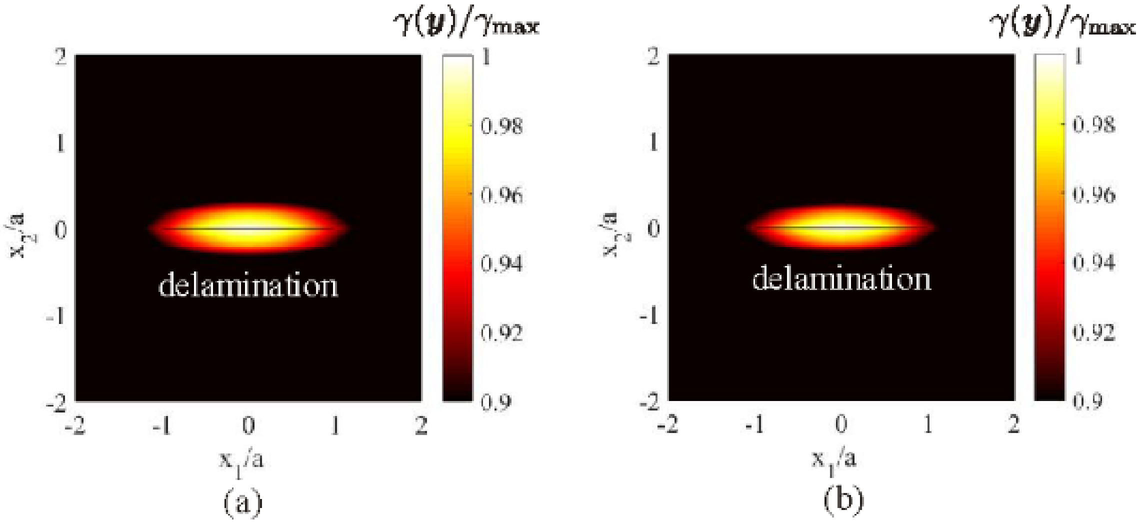


**Figure 5 Shape reconstruction results using the proposed inverse scattering technique for the delamination in (a) unidirectional CFRP (b) quasi-isotropic CFRP.**

$c_0 t/a = 0.02$, $N = 2048$, and $\omega_p = \pi$, respectively. Figure 4(a) and (b) show time variation of scattered wave forms at the receiver points, $(r, \theta) = (12a, \theta = 3^{\circ} + 18^{\circ} n\ (n = 0, \ldots, 9))$ in Fig.3(a). The unidirectional and quasi-isotropic CFRPs whose elastic constants are given in eq.(14) and (15) are considered for Fig.4(a) and (b), respectively. The time-domain transformed wave for the Ricker wave defined in eq. (12) is considered for this analysis. We can see that the scattered waves $u_3^{sc}(\boldsymbol{x}, t)$ arrive at different times for each receiver point, as shown in Fig.4, due to the anisotropic property of CFRPs. The shapes of the group velocity curves for both CFRPs are elliptical, which are shown by blue lines in Fig.2, and the group velocity of qS2 (pure SH wave) for horizontal direction is faster than that for vertical one. These scattered wave forms $u_3^{sc}(\boldsymbol{x}, t)$ can be used for the following inverse scattering analysis.

*Inverse scattering analysis results*

The shape reconstruction results by the proposed method are demonstrated in this section. As mentioned before, the scattered wave forms $u_3^{sc}(\boldsymbol{x}, t)$ in time-domain can be obtained by using the CQBEM. However, scattered wave forms $u_3^{sc}(\boldsymbol{x}, \omega)$ in frequency-domain are required for the computation of right-hand side of eq. (13). The scattered wave forms $u_3^{sc}(\boldsymbol{x}, \omega)$ in frequency-domain are calculated by using the Fourier transform of those $u_3^{sc}(\boldsymbol{x}, t)$ in time-domain in this research. Figure 5(a) and (b) show the results for the shape reconstruction of the delamination in unidirectional and quasi-isotropic CFRPs, respectively. The singular function $\gamma(\boldsymbol{y})/\gamma_{max}$, $\gamma_{max}$ is the maximum value of $\gamma$, is plotted around the delamination. The central straight black line in Fig.5 denotes the actual delamination shape and position. The scattered wave forms $u_3^{sc}(\boldsymbol{x}, t)$ at the receiver points $(r, \theta) = (12a, \theta = 3^{\circ} + 18^{\circ} n\ (n = 0, \ldots, 9))$ for the downward incidence and $(r, \theta) = (12a, \theta = 183^{\circ} + 18^{\circ} n\ (n = 0, \ldots, 9))$ for upward incidence, as shown in Fig.3 (a) and (b), respectively, are used for this inverse scattering analysis for the delamination. We can see that the singular function $\gamma(\boldsymbol{y})/\gamma_{max}$ shows large values around the delamination in Fig.5. Therefore, our proposed inverse scattering technique has the potential to realize the identification of an unknown delamination in various types of CFRP with anisotropic property.

## Conclusions

In this study, the inverse scattering technique for the reconstruction of a delamination in CFRP was proposed. The mathematical formulation for the proposed technique was derived, and tested numerically to verify the proposed method by solving the fundamental inverse scattering problem for the delamination in various types of CFRPs. In this study, only the pure SH wave (qS2 wave) was used for the reconstruction of the delamination in CFRPs. Therefore, in the future, we will try to implement the shape reconstruction using the qP wave. In addition, the extension to 3-D problem is also our next challenge.


## Acknowledgements

This work is supported by JSPS KAKENHI (17H0329400) and "Joint Usage/Research Center for Interdisciplinary Large-scale Information Infrastructures"(jh180049) in Japan.


### References


[1] Doctor, S. R., Hall, T. E. and Reid, L.D. (1986) Saft - the evolution of a signal processing technology for ultrasound testing, *NDT Int.*, **19**(3), 163-167.

[2] Colton, D., Coyle, J. and Monk, P. (2000) Recent developments in inverse acoustic scattering theory, *SIAM Review*, **42**(3), 369-414.

[3] Kitahara, M. and Hirose, S. (1998) Elastodynamic inversion of 3D cavity from backscattering data, *Inverse Problems in Engineering Mechanics*, 163-170.

[4] Kitahara, M., Nakahata, K. and Hirose, S. (2002) Elastodynamic inversion for shape reconstruction and type classification of flaws, *Wave Motion*, **36-4**, 443-455.

[5] Nakahata, K., Saitoh, T. and Hirose, S. (2006) 3-D flaw imaging by inverse scattering analysis using ultrasonic array transducer, *Review of Progress in Quantitative Nondestructive Evaluation*, **34**, 717-724.

[6] Saitoh, T., Hirose, S., Fukui, T. and Ishida, T. (2007) Development of a time-domain fast multipole BEM based on the operational quadrature method in a wave propagation problem, *Advances in Boundary Element Techniques VIII*, V. Minutolo and MH Aliabadi, eds., 355-360.

[7] Saitoh, T. and Hirose, S. (2010) Parallelized fast multipole BEM based on the convolution quadrature method for 3-D wave propagation problems in time-domain, IOP Conf. Series: *Materials Science and Engineering* **10**, 012242.

[8] Furukawa, A., Saitoh, T. and Hirose, S. (2014) Convolution quadrature time-domain boundary element method for 2-D and 3-D elastodynamic analyses in general anisotropic elastic solids, *Engineering Analysis with Boundary Elements*, **39**, 64-74.

[9] Maruyama, T., Saitoh, T., Bui, T. Q. and Hirose, S. (2016) Transient elastic wave analysis of 3-D large-scale cavities by fast multipole BEM using implicit Runge-Kutta convolution quadrature, *Computer Methods in Applied Mechanics and Engineering*, **303**, 231-259.

[10] Sedow, A. and Schmerr, L.W. (1986) The time domain elastodynamic Kirchhoff approximation for cracks, the inverse problem, *Wave Motion*, **8**, 15-26.

[11] Auld, B. A. (1990) Acoustic fields and waves in solids, Vol.1,2, R. E. Krieger.

[12] Wang, C.-Y. and Achenbach, J. D. (1994) Elastodynamic fundamental solutions for anisotropic solids, *Geophys. J. Int.*, **118**, 384-392.

[13] Ricker, N. (1953) The form and laws of propagation of seismic wavelets, *Geophys.*, **18**, 10-40.